Thermodynamic properties of liquid gallium from picosecond acoustic velocity measurements

2015 J. Phys.: Condens. Matter 27 275103

(http://iopscience.iop.org/0953-8984/27/27/275103)

IOP Publishing Journal of Physics: Condensed Matter
J. Phys.: Condens. Matter **27** (2015) 275103 (8pp) doi:10.1088/0953-8984/27/27/275103

Thermodynamic properties of liquid gallium from picosecond acoustic velocity measurements

S Ayrinhac, M Gauthier, G Le Marchand, M Morand, F Bergame and F Decremps

Institut de Minéralogie de Physique des Matériaux et de Cosmochimie (IMPMC), Sorbonne Universités–UPMC Université Pierre et Marie Curie Paris 6, CNRS UMR 7590, Muséum National d'Histoire Naturelle, IRD UMR 206, BC 115, 4 place Jussieu, 75252 PARIS Cedex 05 France

E-mail: simon.ayrinhac@impmc.upmc.fr

Received 3 March 2015, revised 17 April 2015
Accepted for publication 28 April 2015
Published 10 June 2015

Abstract

Due to discrepancies in the literature data the thermodynamic properties of liquid gallium are still in debate. Accurate measurements of adiabatic sound velocities as a function of pressure and temperature have been obtained by the combination of laser picosecond acoustics and surface imaging on sample loaded in diamond anvil cell. From these results the thermodynamic parameters of gallium have been extracted by a numerical procedure up to 10 GPa and 570 K. It is demonstrated that a Murnaghan equation of state accounts well for the whole data set since the isothermal bulk modulus B_T has been shown to vary linearly with pressure in the whole temperature range. No evidence for a previously reported liquid–liquid transition has been found in the whole pressure and temperature range explored.

Keywords: picosecond acoustics, liquid gallium, liquid–liquid phase transition, thermodynamical properties, equations of state

(Some figures may appear in colour only in the online journal)

1. Introduction

Currently, the existence of liquid–liquid phase transition (LLPT, i.e. the transition between two liquids with different local structure) is one of the most interesting topics in condensed matter physics [1]. This topic has become attractive since the discovery of a first-order LLPT in elemental phosphorus [2]. LLPT has been also reported in scarce and various compounds such as Ce [3] or Al_2O_3-Y_2O_3 [1, 4]. Several theoretical explanations have been proposed to explain LLPT on a microscopic frame or from a thermodynamic point of view. Many potentials have been used to reproduce LLPT *in silico*, including an anisotropic interaction pair potential (involved in covalent bonded fluids as water-like liquids) [5, 6] or an isotropic soft-core potential with an attractive well [7]. First-order LLPT has been conjectured to produce a downward kink in the melting curve [8]. A smooth maximum in the melting curve can also be explained by a continuous LLPT [8], as described by a two-liquid model [9]. This continuous transition may indicate the existence of a critical point expected in the metastable liquid [1].

In this context, liquid gallium is a promising candidate for having a LLPT, in view of its low melting temperature (302.9 K [10]) and its ability to be metastable in a large domain that goes down to 150 K [11]. In addition, liquid gallium shares some thermodynamic anomalies with water, known to have a first order transition between two amorphous phases [12]. Like water, the solid gallium floats over the liquid [10, 13] and the supercooled liquid possesses a maximum density line at negative pressures [14].

Simulations have predicted that LLPT exists in liquid gallium in the deep supercooled domain and at negative pressures [15–17]. Moreover, LLPT was experimentally detected in confined liquid gallium at temperature around 200 K [18]. Gradual transitions have also been reported by two experimental studies around 300 K and 2 GPa [19, 20] in the stable liquid. These transitions could be linked to a LLPT, but this hypothesis still needs experimental confirmation.

The coexistence of two different liquids in the stable liquid phase can be explained from a structural point of view. It has been suggested [9] that the short-range order in liquid is very similar to the underlying high pressure crystals, but their nature is still controversial. According to first-principles molecular dynamics, the gallium liquid phases should be linked to Ga-II and Ga-III structures [21]. However, the analysis of structural experimental data have shown that Ga-I and Ga-II are probably the structures involved [22], which shed some confusion on the existence, or not, of LLPT in Ga. Moreover the modifications of the local structure in liquid gallium under high pressure remains poorly understood despite numerous studies [23, 24], the complex character of liquid being due to a possible local anisotropy. Many simulations suggest a mixed covalent and metallic character in the liquid state due to the presence of short-lived Ga_2 dimers [25–28]. These dimers can be considered as a remnant of the Ga-I solid phase since Ga-I is often considered as a quasi-molecular crystal phase [26], with a mix of covalent and metallic bonding. However the existence of the Ga_2 dimers is still questioned [21–23].

The discussion on a possible LLPT in gallium is thus obfuscated and the lack of precision on the determination of the equation of state is one of the most important reasons. The density at high pressure has been obtained by various techniques [13, 20, 24, 29, 30] which exhibit large discrepancies. To clarify this fundamental point, the sound velocity is used in this work as it is known to be a sensitive probe to reveal an eventual phase transition [31]. In section 2 the experimental set-up is described [32]. Sound velocity is reported up to 10 GPa and 570 K in section 3. Then, the thermodynamic properties are determined from sound velocities measurements by a numerical procedure that has previously demonstrated its accuracy and robustness [32–34]. On the basis of these results the remaining question of LLPT in Ga is finally discussed in section 4.

2. Experimental set-up and data analysis

Picosecond acoustics technique is a pump-probe optical method which allows to measure acoustic properties of micrometric samples [32, 35–38]. The experimental set-up was previously described in details in the [32]. The pump and probe laser beams are obtained from the same Ti:sapphire laser with a 79.7 MHz repetition rate. The pump beam is modulated by an acousto-optic modulator and is focused on the surface of the sample. The probe beam is delayed with respect to the pump by a mechanical delay line. The sample surface is imaged through an objective mounted on a piezoelectric device which scan up to a $100 \times 100\,\mu m^2$ region. The pump light is absorbed by the sample and produces via the thermoelastic generation acoustics waves which are detected on the opposite side of the sample. The probe detects the variations of reflectivity which account for the variations in refractive index and surface displacements when the acoustic wave hits the surface. Lock-in measurements are performed to reveal the signal induced by the pump modulation.

A membrane diamond anvil cell (DAC) is used as the high pressure generator and is embedded in a resistive furnace

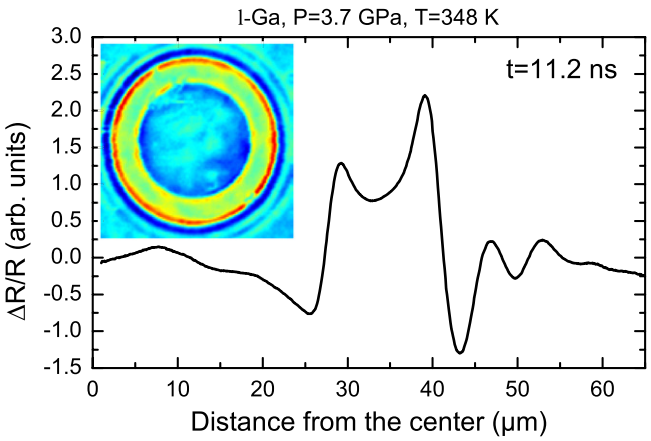

Figure 1. (Inset) experimental image of the acoustic wavefront appearing at the surface of liquid Ga, for a pump-probe delay of $t = 11.2$ ns (the reflectivity is coded with an arbitrary color scale). The main figure shows the integrated profile of the picture.

to reach high temperatures. To measure both pressure and temperature SrB_4O_7:5%Sm^{2+} and ruby chips sensors are used *in-situ*. The pressure is determined by the shift of the SrB_4O_7:5%Sm^{2+} fluorescence line which is known to be temperature independent [39] with an accuracy of 0.1 GPa. Knowing the pressure, the temperature is determined through the power calibration of the furnace and cross checked to the shift of the ruby fluorescence line [40]. The relative uncertainty on the temperature is estimated to be around 1%. The maximum temperature is limited by our heating apparatus and the possible failure of the objectives closed to the heat source.

Gallium (of chemical purity 99.99%) from Sigma-Aldrich is used during the whole set of experiments. Gallium is known to corrode many materials, especially at high temperatures [41], rhenium is thus used as material gasket. This refractory metal is known to remain chemically inert with liquid gallium [42]. While exposed to atmosphere an oxide layer grown on the gallium liquid surface [43]. This oxide layer is removed in HCl 1M [44] and the ultra-pure Ga was then loaded under inert atmosphere inside a glove box. No differences were observed between this sample and the others. This demonstrates that the oxide layer do not disturb the generation and the propagation in the bulk as expected if the oxide layer is very thin compared to the size of the sample [45].

Measurements are carried out using two methods [32, 46]. In the temporal method pump and probe beams are static and collinear and the sample reflectivity is obtained versus the pump-probe time delay. An echo (mostly peak shaped) is observed when the acoustic waves reach the diamond/sample interface. The temporal method measures the transit time Δt of the acoustic pulse propagating through the sample. This method is very efficient and the transit time is obtained in few seconds with an accuracy around 0.1%. In the imagery method the probe beam scans the surface for a chosen pump-probe time delay (figure 1). In isotropic media the wavefront appears as a ring when it reaches the surface. The evolution of the rings radius as a function of time [32, 46] shown in the figure 2 allows to measure independently the sound velocity v

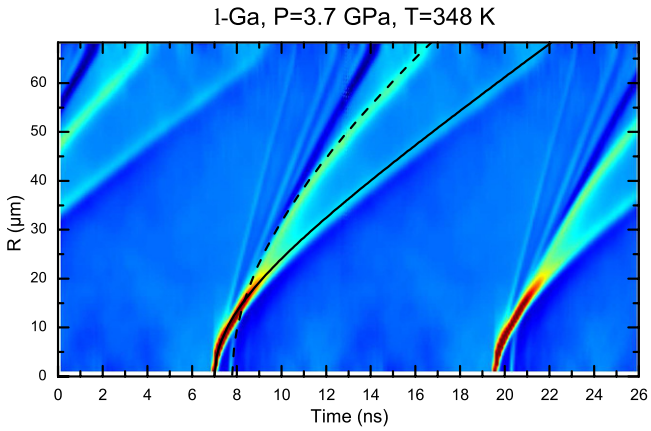

Figure 2. Integrated profiles as a function of time at 3.7 GPa and 348 K. The time scale, limited by the delay line, is extended by repetition of the same picture each T_{laser}. The ripples in this picture highlight the growing of circular wavefronts on the surface of the sample. The evolution of the main wavefront radius is fitted with equation (A.3) (continuous line) while the evolution of the reflected wavefront is calculated (dotted line). The ripples growing linearly with time correspond to surface skimming bulk waves [32].

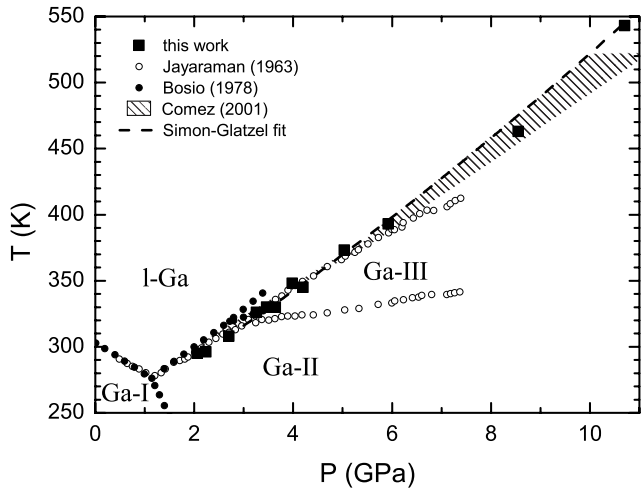

Figure 3. Phase diagram of gallium. The dashed region shows the large uncertainty of the the liquid(l-Ga)-Ga(III) melting curve from Comez [50]. The bold dashed line is a Simon–Glatzel equation (see text) fitted to our data (black squares) above the triple point Ga-II/Ga-III/l-Ga. Other symbols are reported from the literature: Jayaraman [48] (open circles) and Bosio [49] (black circles).

and the thickness e. However this method is time consuming, about 3 h for one measurement. In this study, the sample thickness around 30 μm is chosen in order to balance between accuracy and absorption losses. Using this thickness the diffraction effects neglected in [32] are observable and must be taken into account. The formulas governing the evolution of the radius as a function of time $R(t)$ are detailed in the appendix A. These two complementary methods have been here combined to measure the sound velocity. At each given temperature, measurements were performed by decreasing the pressure from the high pressure to the ambient pressure P_0. A simple linear interpolation of the thickness obtained by the imagery method is used and provides a reliable estimate of the thickness variation as a function of pressure for the whole pressure and temperature range of the experiments since it has been shown that the thickness is weakly pressure dependent during pressure down-stroke (see figure 10 in [47]).

3. Results

3.1. Melting curve

The phase diagram of Ga in its stable phases [48–50] is shown in the figure 3. The sound velocity is a highly sensitive probe to detect the phase transitions, as recently demonstrated in the case of tin by Xu [31]. The temporal method allows to measure the transit time of the echo with a very good accuracy as shown in figure 4 for the liquid–solid transition at 3.3 GPa and 326 K. Present data (figure 3) agree with the melting curve measured by Jayaraman [48] at low pressure ($1 < P < 4$ GPa) and by Comez [50] at high P ($P > 5$ GPa). The melting curve at the liquid-Ga(III) transition can be fitted using a Simon–Glatzel equation [51, 52]

$$T = T_t \left[\frac{P - P_t}{a} + 1 \right]^{\frac{1}{c}} \quad (1)$$

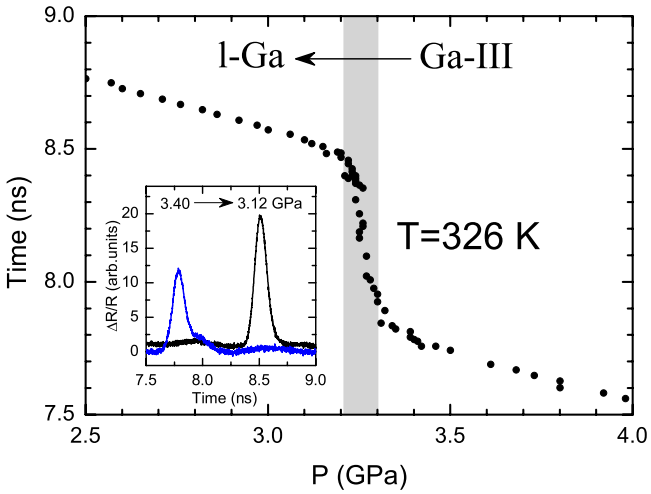

Figure 4. Phase transition between Ga-III and l-Ga observed at 326 K and 3.3 GPa. The shift of the temporal signal observed in the transition zone (in grey) is plotted in the inset.

where the fit parameters are $a = 24$ GPa and $c = 0.51$. The parameters $P_t = 3$ GPa and $T_t = 316$ K correspond to the triple point liquid-Ga(II)-Ga(III) [48]. This new determination of the melting line at high temperature reduces the large uncertainty at the transition liquid-Ga(III) coexistence zone [50].

3.2. Sound velocity measurements

The adiabatic sound velocity v_S in liquid gallium as a function of pressure and for several isotherms is shown in figure 5. The variation of the sound velocity as a function of temperature is very weak so the isotherms are plotted separately for clarity. During the whole experiment, the thickness used in the different runs lay between 18 and 28 μm.

At ambient conditions v_S is determined using the temporal method. Liquid gallium is placed between two sapphire plates

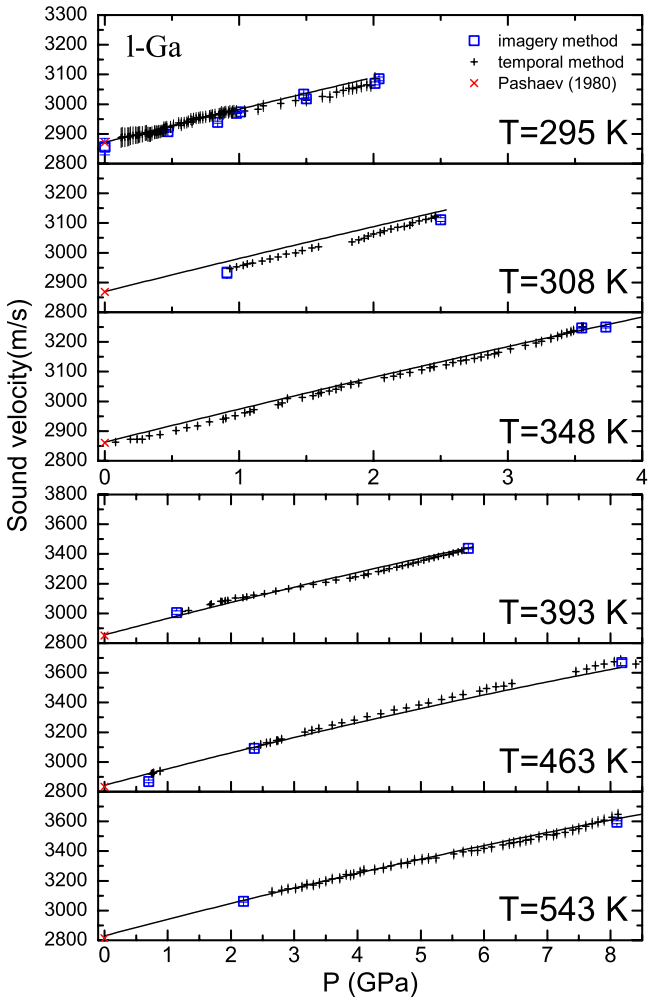

Figure 5. Sound velocity in liquid gallium as a function of pressure at various temperatures, obtained using the temporal (plusses) and the imagery (open squares) methods. The sound velocities at ambient pressure (red crosses) are extracted from Pashaev [53]. Experimental data are fitted with an *ad hoc* polynomial function (see text).

and loaded into a pit drilled into one of the plates using a fast ion beam (FIB). The thickness and the roughness of the pit are measured using conventional atomic force microscopy technique (AFM). The pit method has been used in a previous work [54]. Present measurements were performed with a two-steps pit (depth 1.020 μm/ 6.515 μm) with a surface roughness around $\pm$14 nm. The sound velocity obtained $v_S = 2870 \pm 10\,\mathrm{m\,s^{-1}}$ is in good agreement with the literature data [41, 55].

During down-stroke the crystallization to Ga-I below the melting line is avoided and the gallium remains in a metastable liquid state [55]. The velocity variations are considered smooth in the P–T range explored here. Present data do not show any kink on the P–T range explored here that could be related to a possible LLPT. The sound velocities can be fitted by a simple polynomial expression $v_S(P,T) = v_S^0(1+aT)[1+b(1+cP)P]$ with $v_S^0 = 2923\,\mathrm{m\,s^{-1}}$ and where the TP terms have been neglected since $a = -5.8\ 10^{-5}\,\mathrm{K^{-1}}$, $b = 3.87\ 10^{-2}\,\mathrm{GPa^{-1}}$ and $c = -1.72\ 10^{-2}\,\mathrm{GPa^{-1}}$.

3.3. Thermodynamic properties

The density as a function of pressure and temperature can be extracted from the sound velocity measurements using exact thermodynamic relations [33, 34]. The adiabatic sound velocity v_S is related to the adiabatic compressibility $\beta_S = 1/\rho v_S^2$ and to the thermal compressibility β_T by

$$\beta_T = \frac{1}{\rho}\left(\frac{\partial \rho}{\partial P}\right)_T = \beta_S + \frac{T\alpha_P^2}{\rho\, C_P}, \tag{2}$$

where C_P is the isobaric heat capacity per unit mass and α_P is the thermal expansion coefficient at constant pressure defined by

$$\alpha_P = -\frac{1}{\rho}\left(\frac{\partial \rho}{\partial T}\right)_P. \tag{3}$$

Moreover the isothermal derivative of C_P with respect to P can be written

$$\left(\frac{\partial C_P}{\partial P}\right)_T = -\frac{T}{\rho}\left\{\left(\frac{\partial \alpha_P}{\partial T}\right)_P + \alpha_P^2\right\}. \tag{4}$$

Equations (2)–(4) are used into a recursive procedure adapted from [34] and previously described in detail elsewhere [32] in order to obtain the density, the thermal expansion and the specific heat as a function of pressure and temperature. In addition with $v_S(P,T)$, the knowledge of $\rho(P_0,T)$, $\alpha_P(P_0,T)$ and $C_P(P_0,T)$ (where P_0 notes the ambient pressure) are required. In this work the density $\rho(P_0,T)$ is taken from the polynomial formula given by Hoather [56]. The thermal expansion $\alpha_P(P_0,T)$ is deduced from $\rho(P_0,T)$ by the equation (3). The heat capacity $C_P(P_0,T)$ in $\mathrm{J.kg^{-1}.K^{-1}}$ is obtained from the second order polynomial function given by Chen [57] (T is in K): $C_P(P_0,T) = 496.6 - 0.37\,T + 3\,10^{-4}\,T^2$.

The uncertainties have been evaluated by the introduction of small perturbations in the three input quantities $v(P,T)$, $\rho(P_0,T)$ and $C_P(P_0,T)$. It is observed that the uncertainty increases linearly with P due to the numerical scheme. In the following, the uncertainties are given at 10 GPa. An increase or a decrease of the sound velocity data by $20\,\mathrm{m\,s^{-1}}$ leads to a variation of $\pm$0.15% of the density and $\pm$0.4% of the thermal expansion. The relative uncertainty in $\rho(P_0)$ [56] is roughly $2.6\ 10^{-5}$ which produces relative variations of $\pm 3\ 10^{-5}$ for α_P. According to Chen [57], the heat capacity $C_P(P_0,T)$ is known at $\pm$1.4%. This error dominates the other sources of uncertainties. This leads to relative variations of $\pm 1.5\ 10^{-4}$ for ρ and $\pm 4\ 10^{-4}$ for α_P. All these different uncertainties are quadratically summed and the final maximal uncertainties associated with the absolute measurements of the different quantities at 10 GPa are around $\pm$0.22% for the density, $\pm$0.4% for the thermal expansion and $\pm$1.4% for the heat capacity. Finally the knowledge of the equation of state and $\partial C_P/\partial T$ allows to determine the Gibbs energy function $G(P,T)$ and by derivation the thermodynamic properties of the fluid [58]. Table 1 summarizes the thermodynamic data obtained by this procedure.

In figure 6 the density is plotted as a function of pressure and temperature up to the melting line determined using equation (1). Our data are in excellent agreement with

Table 1. Thermodynamic properties of liquid Ga up to 573 K and 10 GPa.

T (K)	P (GPa)	ρ (kg m^{-3})	α_P (10^{-4} K^{-1})	β_S (10^{-2} GPa^{-1})	B_S (GPa)	β_T (10^{-2} GPa^{-1})	B_T (GPa)
293	0.4	6155	1.24	1.91	52.4	2.08	48.0
293	1.0	6230	1.18	1.80	55.5	1.96	51.0
323	0.0	6079	1.25	2.00	50.0	2.20	45.4
323	1.0	6208	1.16	1.82	55.1	1.98	50.4
323	2.0	6326	1.08	1.66	60.3	1.80	55.5
323	3.0	6436	1.02	1.53	65.5	1.65	60.6
373	0.0	6042	1.21	2.02	49.4	2.25	44.5
373	1.0	6173	1.12	1.84	54.5	2.02	49.4
373	2.0	6293	1.05	1.68	59.6	1.84	54.4
373	3.0	6404	0.99	1.54	64.8	1.68	59.5
373	4.0	6508	0.93	1.43	70.0	1.55	64.6
373	5.0	6606	0.88	1.33	75.3	1.43	69.7
423	0.0	6006	1.17	2.05	48.8	2.29	43.6
423	1.0	6138	1.09	1.86	53.9	2.06	48.5
423	2.0	6260	1.02	1.70	59.0	1.87	53.5
423	3.0	6373	0.96	1.56	64.2	1.71	58.5
423	4.0	6479	0.91	1.44	69.4	1.57	63.6
423	5.0	6577	0.86	1.34	74.6	1.46	68.7
423	6.0	6670	0.82	1.25	79.8	1.36	73.8
473	0.0	5972	1.15	2.07	48.3	2.34	42.8
473	1.0	6105	1.06	1.88	53.3	2.10	47.6
473	2.0	6229	1.00	1.71	58.4	1.90	52.5
473	3.0	6343	0.94	1.57	63.5	1.74	57.5
473	4.0	6450	0.88	1.46	68.7	1.60	62.6
473	5.0	6549	0.84	1.35	73.9	1.48	67.6
473	6.0	6644	0.80	1.26	79.1	1.38	72.7
473	7.0	6732	0.76	1.19	84.3	1.29	77.8
473	8.0	6817	0.73	1.12	89.5	1.21	82.8
523	0.0	5938	1.12	2.10	47.7	2.38	42.0
523	1.0	6073	1.04	1.90	52.7	2.14	46.8
523	2.0	6198	0.97	1.73	57.7	1.94	51.7
523	3.0	6314	0.91	1.59	62.9	1.77	56.6
523	4.0	6422	0.86	1.47	68.0	1.62	61.6
523	5.0	6522	0.82	1.37	73.2	1.50	66.7
523	6.0	6617	0.78	1.28	78.4	1.39	71.7
523	7.0	6707	0.74	1.20	83.6	1.30	76.8
523	8.0	6792	0.71	1.13	88.7	1.22	81.8
523	9.0	6873	0.68	1.07	93.8	1.15	86.8
523	10.0	6951	0.65	1.01	98.8	1.09	91.7
573	0.0	5905	1.10	2.12	47.1	2.43	41.2
573	1.0	6042	1.02	1.92	52.1	2.17	46.0
573	2.0	6168	0.95	1.75	57.2	1.97	50.9
573	3.0	6285	0.90	1.61	62.3	1.79	55.8
573	4.0	6394	0.85	1.48	67.4	1.65	60.8
573	5.0	6496	0.80	1.38	72.6	1.52	65.8
573	6.0	6592	0.76	1.29	77.7	1.41	70.8
573	7.0	6683	0.73	1.21	82.9	1.32	75.8
573	8.0	6769	0.69	1.14	88.0	1.24	80.8
573	9.0	6850	0.67	1.07	93.0	1.17	85.7
573	10.0	6928	0.64	1.02	98.0	1.10	90.6

Note: The uncertainties are discussed in the text.

the data from Köster [29] up to 0.25 GPa. According to the authors the density was determined in a high pressure autoclave with an accuracy of $\pm 3\ 10^{-4}$. Other determinations obtained by various techniques exhibit large and incompatible discrepancies [13, 20, 24, 30]. These discrepancies possibly come from the indirect technique used to determine the density and the necessary underlying hypotheses. Our data do not exhibit the variation of the slope in the relative volume variation, as detected by Li [20] at 330 K and 2 GPa. The density determination from Tamura [30] as a function of T up to 700 bars shows that the slope $\partial\rho/\partial P$ is zero near 300 K and increases with the temperature. Although the uncertainties of the experimental points are quite high, this overall behavior disagrees with our data, where $\partial\rho/\partial P$ is almost independent of the temperature.

Another derived quantity is the isothermal bulk modulus $B_T = \beta_T^{-1}$ shown in the figure 7. Our data agree qualitatively with Lyapin results [13] obtained at 285 K, but the slope of $B_T(P)$ is lower than ours. The value $B_T(P_0) = 12.1(6)$ GPa at 300 K given by Yu [24] seems largely underestimated as for all

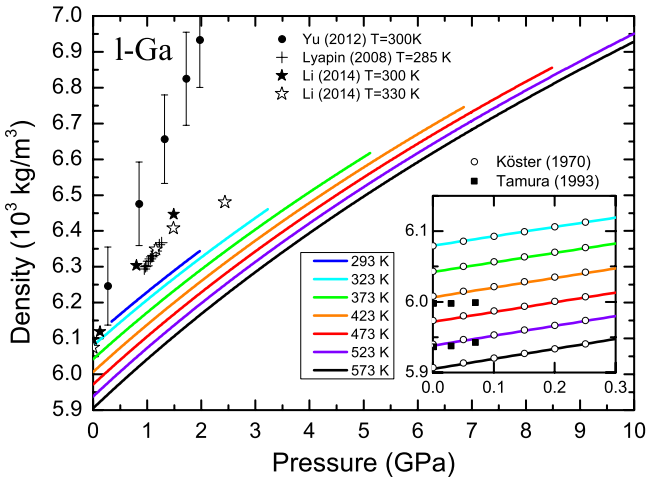

Figure 6. Density ρ of liquid Ga as a function of pressure at different temperatures deduced from present v_S measurements. The data from Yu [24], Lyapin [13] and Li [20] show large discrepancies. (Inset) Comparison between our results and the data from Köster [29] and Tamura [30].

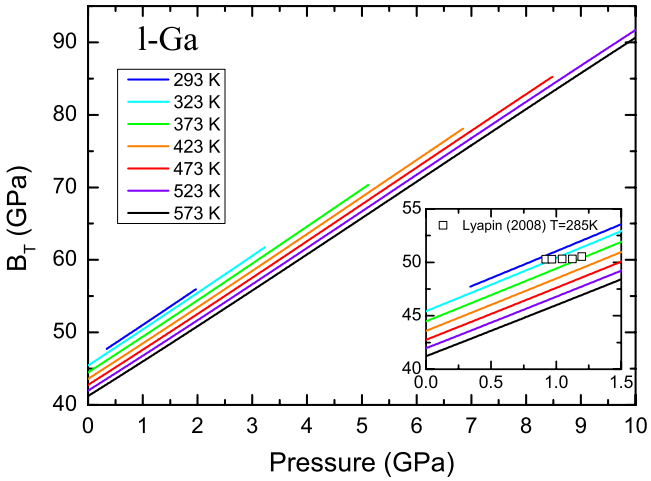

Figure 7. Isothermal bulk modulus B_T as a function of pressure at different temperatures. (Inset) Bulk modulus at low pressures showing the data from Lyapin [13] (empty squares).

other values ($B_T(P_0) = 23.6(0.5)$ GPa at 300 K and $B_T(P_0) = 24.6(0.4)$ GPa at 330 K) presented by Li [20]. The value of β_S at ambient temperature (see table 1) agrees well with the data from Inui [59] which are around $\beta_S = 2.0\ 10^{-2}$ GPa^{-1}.

4. Discussion

Many empirical equations of state (EOS) have been previously proposed to represent the thermodynamic properties of solids [52]. However compared to solids few equations have been used for liquids, as the Tait EOS [60], or the Kumari-Dass EOS for liquid metals [61]. In a previous work [32] we have shown that the EOS for solids can be used for liquids and the Birch–Murnaghan EOS was successfully applied to liquid mercury [32].

Taken into account the accuracy of our numerical procedure, the pressure dependence of bulk modulus B_T is found to be linear (see figure 7) and can be described up to 10 GPa as

$$B_T(P) = B_0 + B_0' P \tag{5}$$

where $B_0 = B_T(P_0)$ and $B_0' = \frac{\partial B_T}{\partial P}(P_0)$. B_0' is found experimentally nearly constant in the P–T range studied with $B_0' = 4.9 \pm 0.2$. This implies that the Murnaghan EOS [52]

$$\rho = \rho_0 \left[1 + \frac{B_0'}{B_0} P\right]^{1/B_0'} \tag{6}$$

is well adapted for the description of liquid Ga. It is straightforward to interpret the Murnaghan EOS as the result of a particular form of the interatomic potential [52] such as Mie potential $\Phi(r) = \frac{a}{r^n} - \frac{b}{r^m}$ with $n > m$ and $r = V^{1/3}$. In liquid metals, the attractive term is modulated by Friedel oscillations due to electron screening and can be written $\cos(2k_F r)/r^3$, where k_F is the Fermi radius sphere [62]. In this simple scheme, from the value of $B_0' = \frac{1}{3}(m + n + 6)$ we can deduce the repulsive term $n = 5.7$. This soft repulsive core agrees well with the interatomic pair potential proposed by Tsai [23] which argues against the description of liquid gallium as a hard spheres liquid.

The Friedel oscillations induce an oscillatory behavior in the interatomic potential leading to the existence of many wells. This complex form of the potential can produce two characteristic interatomic lengths which can be involved in the existence of a LLPT. However at high pressure the repulsive term becomes dominant and the complx long-range attractive term becomes negligible.

Clues for a LLPT around 300 K and 2 GPa was reported in previous experimental studies. A gradual transition was detected by x-ray absorption spectroscopy at 295 K below 2 GPa by Poloni [19], possibly related to a change of the local structure. In the same P–T range a transition was reported by x-ray microtomography technique by Li [20]. In this case an abnormal compressibility of the melt is detected by a variation of the slope in the relative volume variation (empty stars in figure 6). The smooth variations of the sound velocities observed in figure 5 advocate for the absence of phase transition or cross-over in this (P, T) range. If a transition occurs it cannot be differentiated with the normal liquid changes under high P and T. Evidences from simulations [15–17] and experiments [18] claim the LLPT to be expected at low temperature in the deep metastable regime.

As a conclusion, accurate thermodynamic data were obtained in liquid gallium and compared with the literature data. In the P–T domain up to 8 GPa and 540 K for stable liquid gallium no transition was detected in contradiction with recent claims. A liquid–liquid transition would rather be expected in the supercooled liquid regime around 200 K.

Acknowledgments

Authors acknowledge G Ona-Nguema and J Brest for their help with the glove box, N Dumesnil and I Saindou for manufacturing the mechanical parts, I Esteve and S Charron for the MEB characterization and FIB sapphire etching, and J Biscaras for his help on the AFM.

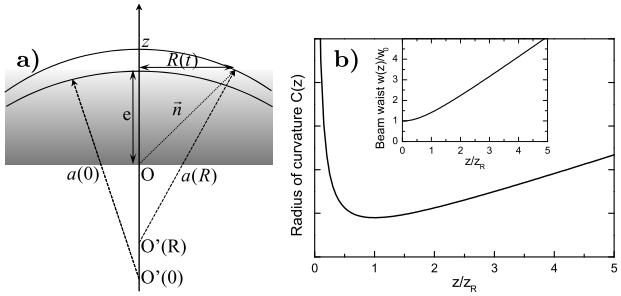

Figure A1. (a) Lateral view of the sample (the physical quantities are discussed in the text). (b) Curvature radius of the wavefront as a function of axial distance z from the point source normalized to the Rayleigh length z_R. (Inset) Radius of the Gaussian acoustic beam.

Appendix A. Diffraction

Acoustic waves are generated at the sample surface by the thermoelastic conversion of the laser pump absorption [37]. These waves move through the sample as a wave packet with a broad frequency range up to THz. They finally hit the opposite side of the sample where they are detected through the intensity variations of the reflected beam probe. The mean frequency of this wave packet is obtained by the Fourier transform of the echo detected in the probe signal (see the left echo in the inset of figure 4) and found to be around few GHz. The typical mean acoustic wavelength λ_{ac} is then around a few μm.

The excited region can be considered as an acoustic Gaussian transducer with a lateral extension given by two times the laser waist w_0 of the pump beam. When the diameter of the Gaussian transducer is large compared to the mean acoustic wavelength only plane waves are detected. However when the focus spot diameter of the laser pump is reduced the diameter of the Gaussian transducer can be decreased down to few μm. Then diffraction effects can be observed on the acoustic waves while the emitted acoustic wavelength is of the same order or larger than the emitter size.

This appendix summarizes the transformations required in the classical mathematical expressions used up to now for the data reduction in the picosecond experiments [32]. These corrections are introduced in the diffraction regime and allow to follow continuously the radius R of the rings observed in surface imagery from the near-field to the far-field approximation.

In the far-field region, the wavefronts are spherical and the source point is the emitter itself. In the near-field region, the source can no longer be considered as a source point. The diffracted waves are nearly planes and behave as if they are emitted by a source rejected at a long distance.

An acoustic wave generated by the laser pump in point O on figure A1(a) reaches the opposite surface of the sample of thickness e at time t_0 and seems to originate from the point $O'(t_0) = O'(0)$. At time t, the acoustic wave generated by the same laser pump pulse has traveled through the sample along the direction $\vec{n}$ but seems to originate from a different source point $O'(t) = O'(R)$. This can be summarized by the two following equations:

$$a^2(R) = R^2 + \left[OO'(R) + e\right]^2, \qquad (A.1a)$$

$$a(R) = z + OO'(R). \qquad (A.1b)$$

Using the same formalism for the acoustic wave generation and propagation than the Gaussian optic formalism used for the laser pump itself (see for example [63]) , we can extract the variation of curvature radius $C(z)$ of the acoustic wave during their propagation in the sample along the z-axis perpendicular to the sample surface (see figure A1(b))

$$C(z) = z\left[1 + \left(\frac{z_R}{z}\right)^2\right] \qquad (A.2)$$

where $z_R = \pi w_0^2/\lambda_{ac}$ is the acoustic Rayleigh length, depending on the mean acoustic wavelength λ_{ac} and w_0 the laser waist which is half of the focus spot diameter.

Using equations (A.1)–(A.2) the diameter dependence R of the rings observed in the probe signal can be easily extracted if it is noticed that the curvature of the acoustic wave is constant in the whole space for each time t and can be identified to $C(z)$

$$R^2 = (z^2 - e^2)\left[1 + \frac{2z}{z+e}\left(\frac{z_R}{z}\right)^2\right]. \qquad (A.3)$$

Finally the substitution of $e = v\Delta t$ and $z = vt$ in equation (A.3) leads to the equation given in [32] plus a corrective term depending on z_R. The Rayleigh length z_R depends on the geometry of the experiment. It can be treated as a free parameter in a numerical procedure fitting the experimental curve $R(t)$ since it is not obvious to precisely estimate the size of the focus spot and the acoustic wavelength. In this work we obtained an average value $z_R \simeq 9\,\mu$m, which is compatible with the experimental estimated values of $w_0 \simeq 1.5$–$2.5\,\mu$m and $\lambda_{ac} \simeq 1$–$3\,\mu$m.

References

[1] McMillan P F, Wilson M, Wilding M C, Daisenberger D, Mezouar M and Greaves G N 2007 *J. Phys.: Condens. Matter* **19** 415101
[2] Katayama Y, Mizutani T, Utsumi W, Shimomura O, Yamakata M and Funakoshi K-i 2000 *Nature* **403** 170
[3] Cadien A, Hu Q, Meng Y, Cheng Y, Chen M, Shu J, Mao H and Sheng H 2013 *Phys. Rev. Lett.* **110** 125503
[4] Aasland S and McMillan P 1994 *Nature* **369** 633
[5] Poole P H, Sciortino F, Essmann U and Stanley H E 1992 *Nature* **360** 324
[6] Saika-Voivod I, Sciortino F and Poole P H 2000 *Phys. Rev.* E **63** 011202
[7] Skibinsky A, Buldyrev S V, Franzese G, Malescio G and Stanley H E 2004 *Phys. Rev.* E **69** 061206
[8] Makov G and Yahel E 2011 *J. Chem. Phys.* **134** 204507
[9] Rapoport E 1967 *J. Chem. Phys.* **46** 2891
[10] Mangum B W and Thornton D D 1979 *Metrologia* **15** 201
[11] Bosio L and Windsor C G 1975 *Phys. Rev. Lett.* **35** 1652
[12] Mishima O, Calvert L and Whalley E 1985 *Nature* **314** 76
[13] Lyapin A, Gromnitskaya E, Yagafarov O, Stalgorova O and Brazhkin V 2008 *J. Exp. Theor. Phys.* **107** 818
[14] Imre A, Maris H and Williams P 2002 *Liquids Under Negative Pressure: NATO Science Series* (*Series II: Mathematics, Physics and Chemistry*) (Berlin: Springer)
[15] Carvajal Jara D A, Fontana Michelon M, Antonelli A and de Koning M 2009 *J. Chem. Phys.* **130** 221101

[16] Cajahuaringa S, de Koning M and Antonelli A 2012 *J. Chem. Phys.* **136** 064513
[17] Cajahuaringa S, de Koning M and Antonelli A 2013 *J. Chem. Phys.* **139** 224504
[18] Tien C, Charnaya E V, Wang W, Kumzerov Y A and Michel D 2006 *Phys. Rev.* B **74** 024116
[19] Poloni R, De Panfilis S, Di Cicco A, Pratesi G, Principi E, Trapananti A and Filipponi A 2005 *Phys. Rev.* B **71** 184111
[20] Li R, Li L, Yu T, Wang L, Chen J, Wang Y, Cai Z, Chen J, Rivers M L and Liu H 2014 *Appl. Phys. Lett.* **105** 041906
[21] Yang J, Tse J S and Iitaka T 2011 *J. Chem. Phys.* **135** 044507
[22] Yagafarov O F, Katayama Y, Brazhkin V V, Lyapin A G and Saitoh H 2012 *Phys. Rev.* B **86** 174103
[23] Tsai K H, Wu T-M and Tsay S-F 2010 *J. Chem. Phys.* **132** 034502
[24] Yu T, Chen J, Ehm L, Huang S, Guo Q, Luo S-N and Parise J 2012 *J. Appl. Phys.* **111** 112629
[25] Defrain A 1977 *J. Chim. Phys. Phys.-Chim. Biol.* **74** 851
[26] Gong X G, Chiarotti G L, Parrinello M and Tosatti E 1991 *Phys. Rev.* B **43** 14277
[27] Gong X G, Chiarotti G L, Parrinello M and Tosatti E 1993 *Europhys. Lett.* **21** 469
[28] Huisman W J, Peters J F, Zwanenburg M J, de Vries S A, Derry T E, Abernathy D and van der Veen J F 1997 *Nature* **390** 379
[29] Köster H, Hensel F and Franck E 1970 *Ber. Bunsenges. Phys. Chem.* **74** 43
[30] Tamura K and Hosokawa S 1993 *J. Non-Cryst. Solids* **156** 650
[31] Xu L, Bi Y, Li X, Wang Y, Cao X, Cai L, Wang Z and Meng C 2014 *J. Appl. Phys.* **115** 164903
[32] Ayrinhac S, Gauthier M, Bove L E, Morand M, Le Marchand G, Bergame F, Philippe J and Decremps F 2014 *J. Chem. Phys.* **140** 244201
[33] Davis L A and Gordon R B 1967 *J. Chem. Phys.* **46** 2650
[34] Daridon J, Lagourette B and Grolier J-P 1998 *Int. J. Thermophys.* **19** 145
[35] Thomsen C, Grahn H T, Maris H J and Tauc J 1986 *Phys. Rev.* B **34** 4129
[36] Sugawara Y, Wright O B, Matsuda O, Takigahira M, Tanaka Y, Tamura S and Gusev V E 2002 *Phys. Rev. Lett.* **88** 185504
[37] Wright O B, Perrin B, Matsuda O and Gusev V E 2008 *Phys. Rev.* B **78** 024303
[38] Decremps F, Belliard L, Perrin B and Gauthier M 2008 *Phys. Rev. Lett.* **100** 035502
[39] Datchi F, Dewaele A, Loubeyre P, Letoullec R, Le Godec Y and Canny B 2007 *High Press. Res.* **27** 447
[40] Raju S V, Zaug J M, Chen B, Yan J, Knight J W, Jeanloz R and Clark S M 2011 *J. Appl. Phys.* **110** 023521
[41] Prokhorenko V Y, Roshchupkin V, Pokrasin M, Prokhorenko S and Kotov V 2000 *High Temp.* **38** 954
[42] Hampel C 1961 *Ind. Eng. Chem.* **53** 90
[43] Xu Q, Oudalov N, Guo Q, Jaeger H. M and Brown E 2012 *Phys. Fluids* **24** 063101
[44] Xu Q, Brown E and Jaeger H M 2013 *Phys. Rev.* E **87** 043012
[45] Regan M J, Tostmann H, Pershan P S, Magnussen O M, DiMasi E, Ocko B M and Deutsch M 1997 *Phys. Rev.* B **55** 10786
[46] Decremps F, Gauthier M, Ayrinhac S, Bove L, Belliard L, Perrin B, Morand M, Marchand G L, Bergame F and Philippe J 2015 *Ultrasonics* **56** 129
[47] Dewaele A, Eggert J H, Loubeyre P and Le Toullec R 2003 *Phys. Rev.* B **67** 094112
[48] Jayaraman A, Klement W Jr, Newton R and Kennedy G 1963 *J. Phys. Chem. Solids* **24** 7
[49] Bosio L 1978 *J. Chem. Phys.* **68** 1221
[50] Comez L, Di Cicco A, Itié J P and Polian A 2001 *Phys. Rev.* B **65** 014114
[51] Simon F and Glatzel G 1929 *Z. Anorg. Allg. Chem.* **178** 309
[52] Poirier J-P 2000 *Introduction to the Physics of the Earth's Interior* (Cambridge: Cambridge University Press)
[53] Pashaev B, Palchaev D, Pashuk E and Revelis V 1980 *J. Eng. Phys.* **38** 358
[54] Decremps F, Belliard L, Couzinet B, Vincent S, Munsch P, Le Marchand G and Perrin B 2009 *Rev. Sci. Instrum.* **80** 073902
[55] Proffit R and Carome E 1962 *Technical Report No 5* (Ft. Belvoir, VA: Defense Technical Information Center) www.dtic.mil/dtic/tr/fulltext/u2/274205.pdf
[56] Hoather W 1936 *Proc. Phys. Soc.* **48** 699
[57] Chen H and Turnbull D 1968 *Acta Metall.* **16** 369
[58] Jacobs M H and Oonk H A 2000 *Phys. Chem. Chem. Phys.* **2** 2641
[59] Inui M, Takeda S and Uechi T 1992 *J. Phys. Soc. Japan* **61** 3203
[60] Dymond J and Malhotra R 1988 *Int. J. Thermophys.* **9** 941
[61] Kumari M and Dass N 1990 *J. Phys.: Condens. Matter* **2** 3219
[62] Bove L E, Formisano F, Sacchetti F, Petrillo C, Ivanov A, Dorner B and Barocchi F 2005 *Phys. Rev.* B **71** 014207
[63] Milonni P and Eberly J 2010 *Laser Physics* (New York: Wiley)